The molecular origin of fast water transport in carbon nanotube membranes: superlubricity versus curvature dependent friction

K. Falk, F. Sedlmeier, L. Joly, R. R. Netz, L. Bocquet

June 2010

1 Simulation details

We performed simulations with two different MD simulation packages (LAMMPS and GROMACS) and two different water models (TIP3P and SPC-E). For the oxygen-carbon interaction a Lennard-Jones potential was used with AMBER (for TIP3P) and WERDER (for SPC-E) parameters, respectively. The hydrogen-carbon interaction is neglected. The values of the parameters for the interaction potentials are given in Tab.1. Number of particles, volume and temperature were constant (NVT). The carbon positions were fixed. Water temperature was controled by a Nosé/Hoover thermostat and kept at 300K. The thermostat was coupled only at the velocity components perpendicular to the flow direction.

Below, we concentrate on the results obtained with the TIP3P water model. A discussion of the simulations with the SPC-E water model follows in the last part.

	TIP3P/AMBER	SPC-E/WERDER
d_{OH}(A)	0.9572	1.0
$\sphericalangle HOH$	104.52	109.47
$q_O(e)$	-0.834	-0.8476
$q_H(e)$	0.417	0.4238
σ_{OO}(A)	3.151	3.166
ϵ_{OO}(kJ/mol)	0.636	0.650
σ_{OC}(A)	3.276	3.190
ϵ_{OC}(kJ/mol)	0.477	0.392

Table 1: Water model and interaction parameters

1.1 Pressure control

In order to ensure equal pressure conditions for all simulations, the number of water molecules was previously determined in additional equilibrium simulations with tubes of finite size. For water inside a CNT, reservoirs were added at both open ends of the tube. The reservoirs were kept at 1atm by a piston. For simulations of water outside CNT, the pressure was also imposed by a piston perpendicular to the tube axes. In most of the slab simulations, the number of molecules was fixed arbitrarily, and the volume was adjusted instead to control the pressure: One graphene plane was used as a piston while the second plane was fixed. For the subsequent measurements, the positions of both planes were fixed at the equilibrium distance which was found. This process requires less particles and therefore less computing time than an equilibration with particle reservoirs. This procedure is not suitable for slab sizes $H \lesssim 1.5$nm, where hydrophobic interactions between walls start to become noticeable. If the wall is allowed to move, dewetting may occur and lead to air cavities. Completely water filled graphene slabs of sub nanometer size can be obtained, however, by using particle reservoirs (at 1atm) as for the CNT.

1.2 Normal and tangential pressure

While the tangential pressure $p_{\mathrm{T}} = 1$ atm is the same in all simulations, the normal pressure at the water/carbon interface

$$p_{\mathrm{N}}(R) = p_{\mathrm{T}} - \frac{\gamma_{\mathrm{ls}}}{R} \tag{1}$$

is curvature dependent due to the liquid solid surface tension γ_{ls}. We observed a strong decrease of the normal pressure with the CNT radius, corresponding to a surface tension of $\gamma_{\mathrm{ls}} \approx 0.07 \frac{\mathrm{N}}{\mathrm{m}}$ (Fig.1a).

However, this pressure drop is not responsible for the observed curvature dependence of the friction coefficient. This was checked in graphene slab simulations (Fig.1b) and a CNT of radius $R = 1.02$ nm for tangential pressures between -1000atm and 500atm.

1.3 Density profile and radial potential

The upper plot in Fig.2 shows the potential energy $V(r)$ of one oxygen atom positioned at $(r, \theta = 0, z = 0)$ due to its interaction with all carbon atoms, and the radial density profile of oxygen $\rho(r)$. The oxygen-carbon interaction results in a region of highly increased water density next to the wall (gray background). We refer to this region of molecular thickness as to the "first water layer". From the outside to the inside, the first layer is followed by a second layer and the bulk region. The distance between the first layer and the carbon wall ($\sigma_{\mathrm{OC}} = 0.328$nm) is independent of the CNT radius. For decreasing tube radii down to $R \approx 1$nm, the potential well deepens slightly (lower right plot) which consequently leads to an equally slight increase of the contact density (lower

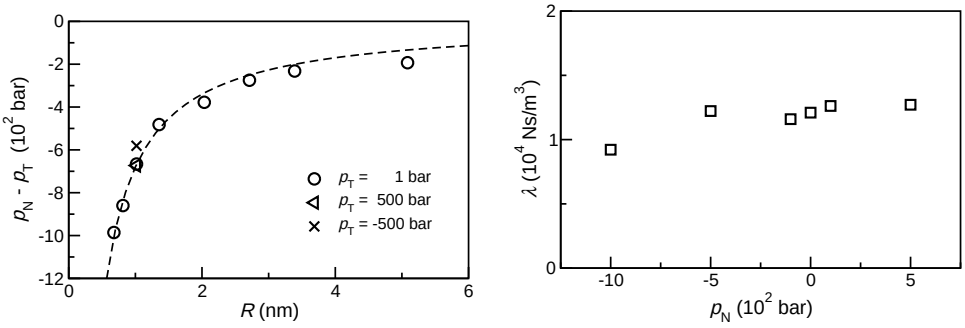

(a) Influence of curvature on normal pressure

(b) Independence of friction on pressure

Figure 1: *(a)* Difference of normal and tangential pressure in a CNT of radius $R = 1.02$nm. For increasing curvature the pressure normal to the CNT wall is reduced about $10^2 - 10^3$atm due to the liquid-solid surface tension. A fit $p_{\mathrm{N}}(R) - p_{\mathrm{T}} = -\frac{\gamma_{\mathrm{ls}}}{R}$ (dotted line) gives $\gamma_{\mathrm{ls}} \approx 0.07\frac{\mathrm{N}}{\mathrm{m}}$ for the water graphene surface tension. *(b)* Friction coefficient λ for water in a graphene slab ($H \approx 2.5$nm) for varying pressure. For pressure between $[-1000;\ 500]$atm, no change in friction was observed. Therefore, the pressure drop at the CNT wall due to surface tension can not explain the observed curvature dependence of the friction coefficient.

left). For even smaller radii $R < 1$nm, the potential well deepens considerably. The small diameter allows only for four water molecules or less. These tubes do not contain bulk water.

In the following, we concentrate on the weak confinement regime $R > 1$nm and discuss the strong confinement regime $R < 1$nm afterwards.

2 Weak confinement

2.1 Depletion length

The layering of a fluid near a plane wall can be quantified by the depletion length δ, which is defined as the integrated density variation. For a graphene slab with carbon positions $z = \pm\frac{H}{2}$, the depletion length is

$$\delta_{\mathrm{planar}} = \frac{1}{2}\int_{-\frac{H}{2}}^{\frac{H}{2}} dz\ \left(1 - \frac{\rho(z)}{\rho_{\mathrm{bulk}}}\right) \tag{2}$$

and for a CNT with radius R we define

$$\delta_{\mathrm{zylindric}} = \frac{1}{R}\int_0^R dr\ r\ \left(1 - \frac{\rho(r)}{\rho_{\mathrm{bulk}}}\right). \tag{3}$$

The bulk region $\rho = \rho_{\mathrm{bulk}}$ should give zero contribution to the depletion length, but in practice, statistical density fluctuations in MD simulations add to the

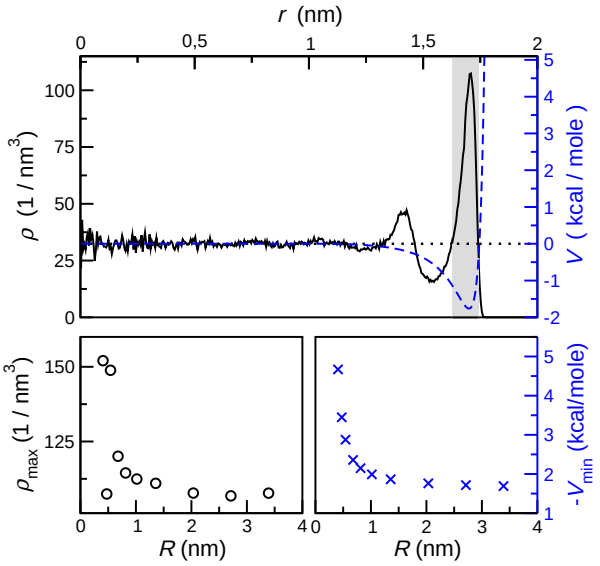

Figure 2: Density profile and potential for TIP3P water in armchair CNT. *Upper plot*: radial density function of oxygen and potential energy $V(r)$ of one oxygen atom positioned at $(r; \theta = 0, z = 0)$ for $R = 2.03$nm. The contact density increases along with the curvature (*lower left*) due to the deepening of the potential well (*lower right*).

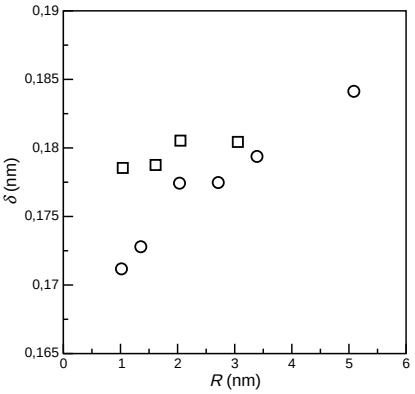

Figure 3: Depletion length of water in graphene slabs of size $H = 2R$ ($\square$) and of water in CNT with radius R ($\circ$) - see Eq (2) and (3)

result. To reduce the impact of fluctuations, we did not include the bulk region in the calculation of the depletion length. The values we thus get for the depletion length with the bulk density $\rho_{\text{bulk}} = 32.4$ molecules/nm^3 are shown in Fig.3.

We do not observe the expected relation $\lambda \sim \delta^{-4}$between the friction coefficient and the depletion length. Instead of increasing, the depletion length decreases slightly with the CNT radius (less than 10% in the range from 5 to 1nm). Furthermore, the result for tubes of big diameter do not match the result for graphene, which would be expected when the curvature gets small. Finally, the depletion length is not a good parameter to characterize the water CNT interaction for $R < 1$nm because no bulk density can be defined.

2.2 Flow measurement of the friction coefficient

In flow simulations, the friction coefficient was determined directly from

$$\lambda = -\frac{F/A}{v_{\text{slip}}} \tag{4}$$

by measuring the friction force F and the slip velocity v_{slip} for different flow velocities. The contact area $A = 2\pi r_{\text{eff}} L$ between water and CNT (inside and outside) is calculated with the effective radius $r_{\text{eff}} = R \mp \frac{1}{2}\sigma_{\text{OC}}$.

The water flow was driven by a constant acceleration. Instead of the expected parabolic Poiseuille flow, we found a constant velocity profile. This implies a large slip length $b \gg R$ ($b \gg H$), which means low friction. Due to the low friction, the system needs a long time to reach the stationary state $v_{\text{stationary}} = F_{\text{extern}}/\lambda A$. But to determine the friction coefficient λ, the system does not necessarily have to be in a stationary state. On the contrary, the evolving flow allows to trace the dependence of the friction force on the velocity $F(v_{\text{slip}})$ for the complete range $0 \leq v_{\text{slip}}(t) \leq v_{\text{stationary}}$ in one single simulation. Due to the constant velocity profile, the slip velocity v_{slip} can be considered as equal

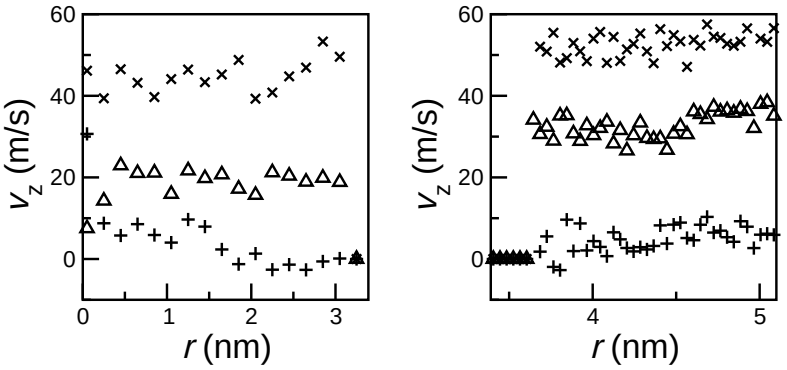

Figure 4: Flow profiles inside (*left*) and outside (*right*) a CNT with radius $R = 3.39$nm. Water was initially at rest and was then accelerated by a constant force. The shown profiles result from time averages over 20 fs, starting 0(+), 0.08(△) and 0.18 ns(×) after switching on the external force.

to the mean velocity of all water molecules instead of only those on the wall. This increases statistics considerably. One example for the time evolution of the velocity profiles is shown in Fig.4.

We used accelerations $\sim 10^{-4} \frac{\mathrm{nm}}{\mathrm{ps}^2}$ to get flow velocities of maximal $50 \frac{\mathrm{m}}{\mathrm{s}}$ (For higher velocities, we note a non-linear dependence of the friction force on the slip velocity). During 0.2 ns, F and v_{slip} were calculated every 2fs (every timestep) and averaged over time intervals of 20fs. The slope of $F(v_{\mathrm{slip}})$ was then determined from a linear fit on the resulting 10 data points. This procedure was repeated for 20 different initial conditions. Finally we obtain the friction coefficient λ from the mean value of the slope.

Fig.1 of the article shows some results for the relation $F(v_{\mathrm{slip}})$. For better visibility, we averaged the original data points (200 for each tube) within certain velocity intervals. The dotted lines represent the results for the friction coefficientλ that we obtained from the described evaluation procedure.

2.3 Green-Kubo formula & force auto correlation function

In equilibrium simulation the friction coefficient was determined according to the Green-Kubo formula

$$\lambda = \frac{1}{k_{\mathrm{B}} T A} \int_0^\infty dt \, \langle F(t) F(0) \rangle \, . \tag{5}$$

Eq. 5 connects the friction coefficient to the auto correlation function of the thermal fluctuations of the friction force F. It was calculated every 2 fs for a duration of 0.4 ns. The ACF (Fig.5a) and its time integral $\int_0^t dt' \, \langle F(t') F(0) \rangle$ were calculated for $t < 2$ps . The friction coefficient was found from a constant fit on the integrated ACF (Fig.5b) in the region $0.6 < t < 2$ ps .

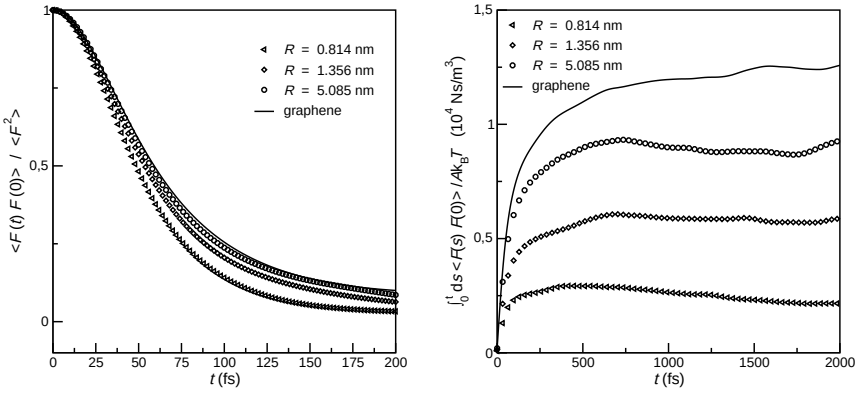

(a) Force auto correlation function

(b) Green-Kubo expression

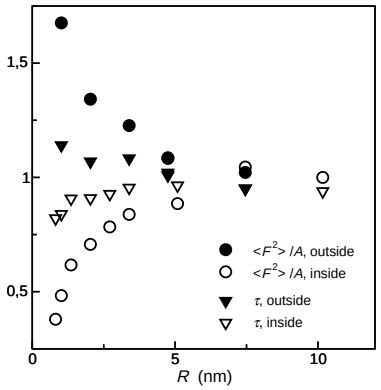

(c) Mean squared force and correlation time

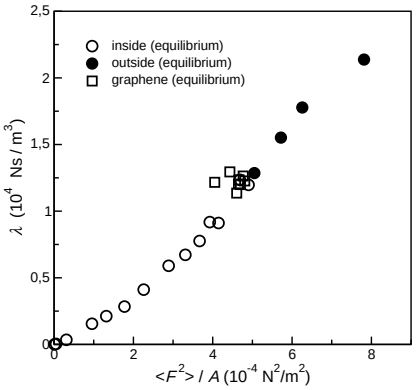

(d) Friction coefficient

Figure 5: *(a)* normalized force ACF $\langle F(t)F(0)\rangle / \langle F^2\rangle$ for water filled CNT of different radii and for water on graphene. *(b)* time evolution of the GK expression $\frac{1}{k_B T A}\int_0^t dt'\ \langle F(t')F(0)\rangle$; the friction coefficient λ was found from a constant fit on the plateau from 0.6 to 2ps. *(c)* radius dependence of the mean squared force per unit area $\langle F^2\rangle / A$ and of the force correlation time τ for water inside and outside of the CNT; normalized on the values for graphene. *(d)* (almost linear) dependence of the friction coefficient on the mean squared force.

In equilibrium systems, the friction coefficient is directly proportional to the integral over the auto correlation function of the fluctuating friction force F. With decreasing radius, the mean squared force changes much stronger than the correlation time, which indicates that the curvature dependence of the friction coefficient is mainly a static effect.

2.4 Correlation time and mean squared force

The curvature dependence of the friction coefficient

$$\lambda \approx \frac{\tau}{k_{\mathrm{B}}T} \frac{\left\langle F^2 \right\rangle}{A} \tag{6}$$

is predominantly a static effect. For weak confinements $R < 1$nm, the force correlation time τ is almost independent of the tube size, whereas the mean squared force shows the same qualitative behavior as the friction coefficient (Fig.5c and 5d). The origin of the curvature dependence becomes clear from a closer look at the potential $V(\mathbf{r})$ of one oxygen atom at position $\mathbf{r}$ due to its interaction with all carbon atoms, since the force can be written as $F = \int \mathrm{d}^3 r \; f(\mathbf{r})$ with $f(\mathbf{r}) = \partial_z V(\mathbf{r})$. Keeping in mind the density profile from Fig.2, we assume that the main contribution to the force comes from the water molecules in the first layer

$$F \approx \int \mathrm{d}z \int \mathrm{d}s \; \partial_z V(r_{\mathrm{O}}, s, z) \tag{7}$$

where $r_{\mathrm{O}} = R \pm \sigma_{\mathrm{OC}}$ is the mean radial position of the water molecules in the first layer (inside or outside the CNT) and $s = r_{\mathrm{O}}\theta$.

2.5 Oxygen-wall potential

From a numerical calculation of the potential $V(s, z)$ for one oxygen atom in the first layer, we see that it has the same periodicity as the projection of the carbon structure on the cylinder with radius r_{O}. The lattice vectors for the projected structure are

$$\begin{aligned} \mathbf{a}_+ &= \frac{l_0}{2} \begin{pmatrix} \sqrt{3}\frac{r_{\mathrm{O}}}{R} \\ 1 \end{pmatrix} \\ \mathbf{a}_- &= \frac{l_0}{2} \begin{pmatrix} \sqrt{3}\frac{r_{\mathrm{O}}}{R} \\ -1 \end{pmatrix} \end{aligned} \tag{8}$$

where $l_0 = \sqrt{3}d$ (carbon-carbon distance $d = 0.142$ nm) is the length of the lattice vectors for the graphene structure which is recovered in the limit $\frac{r_{\mathrm{O}}}{R} \to 1$. The corresponding reciprocal lattice vectors are

$$\begin{aligned} \mathbf{q}_+ &= q_0 \begin{pmatrix} \frac{R}{\sqrt{3}r_{\mathrm{O}}} \\ 1 \end{pmatrix} \\ \mathbf{q}_- &= q_0 \begin{pmatrix} \frac{R}{\sqrt{3}r_{\mathrm{O}}} \\ -1 \end{pmatrix} \end{aligned} \tag{9}$$

where $q_0 = 2\pi/l_0$. The resulting force in z-direction $f = -\partial_z V(s, z)$ on an oxygen atom of the first layer has the same periodicity. The potential $V(s, z)$

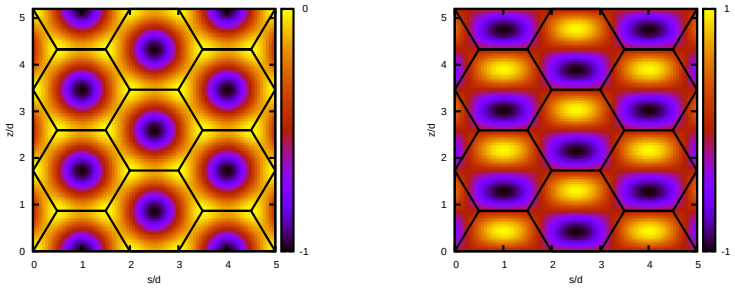

Figure 6: Potential landscape $V(s,z)$ (*left*) and its derivative $\partial_z V$ (*right*) for one oxygen atom at the distance 0.328nm of a graphene plane (distances are normalized by the C-C distance $d = 0.142$nm)

and the derivative $\partial_z V(s,z)$ are shown in Fig.6 for a plane graphene sheet (see also Fig.5 in the article).

From a Fourier analysis, we find that the force is in first approximation

$$f\ (\mathbf{x} = (s,z)) = f_{q_\parallel}\left(\sin(\mathbf{q}_+ \cdot \mathbf{x}) - \sin(\mathbf{q}_- \cdot \mathbf{x})\right) \tag{10}$$

The mean force can therefor be written as

$$\begin{aligned}\left\langle F^2 \right\rangle &= \int \mathrm{d}^2\mathbf{x} \int \mathrm{d}^2\mathbf{x}'\ f(\mathbf{x}) f(\mathbf{x}') \left\langle \rho(\mathbf{x})\rho(\mathbf{x}')\right\rangle \\ &= f_{q_\parallel}^2 \int \mathrm{d}^2\mathbf{x} \int \mathrm{d}^2\mathbf{x}'\ \left(\sin(\mathbf{q}_+ \cdot \mathbf{x}) - \sin(\mathbf{q}_- \cdot \mathbf{x})\right) \times \\ &\qquad \left(\sin(\mathbf{q}_+ \cdot \mathbf{x}') - \sin(\mathbf{q}_- \cdot \mathbf{x}')\right) \left\langle \rho(\mathbf{x})\rho(\mathbf{x}')\right\rangle .\end{aligned}$$

And, by using the relation $\left\langle \tilde{\rho}\left(\mathbf{q}\right) \tilde{\rho}\left(-\mathbf{q}\right)\right\rangle = NS(\mathbf{q})$, we finally get

$$\lambda \sim \frac{\left\langle F^2 \right\rangle}{A} = \frac{1}{2}\frac{N}{A} f_{q_\parallel}^2 \left(S(\mathbf{q}_+) + S(\mathbf{q}_-)\right) = \frac{N}{A} f_{q_\parallel}^2 S(q_\parallel) \tag{11}$$

with the length of the reciprocal lattice vectors $q_+ = q_- =: q_\parallel$. All quantities in the expression above are 1) characteristics of the first water layer and 2) easily accessible in MD simulations. N is the average number of water molecules in the first layer, $f_{q_\parallel}$ is the amplitude of the lateral oxygen potential (see Eq.(10)) and $S(\mathbf{q})$ is the 2-dimensional structure factor of the 'unrolled' first water layer. 'Unrolled' means that the positions of all oxygen atoms in the first layer are mapped according to

$$\mathbf{r} = (r,\ \theta,\ z) \longrightarrow \mathbf{x} = (s\ , z) \tag{12}$$

The structure factor is calculated as follows

$$S(\mathbf{q}) = \frac{1}{N}\left\langle \sum_{j=1}^{N}\sum_{l=1}^{N} \exp(\mathrm{i}\mathbf{q}\cdot(\mathbf{x}_l - \mathbf{x}_j)) \right\rangle \tag{13}$$
$$= \frac{1}{N}\left\langle \left(\sum_{j=1}^{N}\cos(\mathbf{q}\cdot\mathbf{x}_j)\right)^2 + \left(\sum_{j=1}^{N}\sin(\mathbf{q}\cdot\mathbf{x}_j)\right)^2 \right\rangle$$

In the weak confinement regime, the water structure is independent of the **q**-direction and of the tube radius. It is the same as for the fist water layer in a graphene slab (Fig.3 of the article).

2.6 Curvature dependence of roughness, structure and contact density

All three contributions to the mean squared force - contact density $\frac{N}{A}$, roughness $f_{q_\parallel}$ and commensurability factor $S(q_\parallel)$ - depend on the tube radius (Fig.7b). As already mentioned above, higher curvature leads to a slightly deeper potential well at the position of the first water layer and therefore to a higher contact density (Fig.2). Secondly, it smoothens the potential in lateral direction to the wall, so that the force amplitude $f_{q_\parallel}$ decreases. The biggest change with curvature takes place for the structural factor $S(q_\parallel)$. However, this is not due to a change in the water structure. In weak confinement, the structure factor of the first water layer remains unchanged. But the length of the reciprocal lattice vector

$$q_\parallel(R) = \frac{2\pi}{l_0}\sqrt{\frac{R^2}{3r_{\mathrm{O}}^2} + 1} \tag{14}$$

is radius dependent (Fig.7a). Hence, the function $S(q)$ has to be evaluated at another q-value for each tube radius.

3 Strong confinement

With increasing confinement, the water molecules get more and more ordered along the tube axes, up to the point where they build a single file chain for the two smallest tubes ($R = 0.34$ and 0.41nm). Hence an evaluation with the structure factor defined in Eq. (13) is not possible, because the range of the angular coordinate $s = \theta r_{\mathrm{O}}$ becomes too small, from a few molecular diameters to $s \approx 0$ for water arranged in single file. The two dimensional water layer is reduced to a one dimensional chain. To quantify the structuring that occurs hereby, we calculated the structure factor in z-direction:

$$S(q) = \frac{1}{N}\left\langle \sum_{j=1}^{N}\sum_{l=1}^{N} \exp(\mathrm{i}q(z_l - z_j)) \right\rangle \tag{15}$$

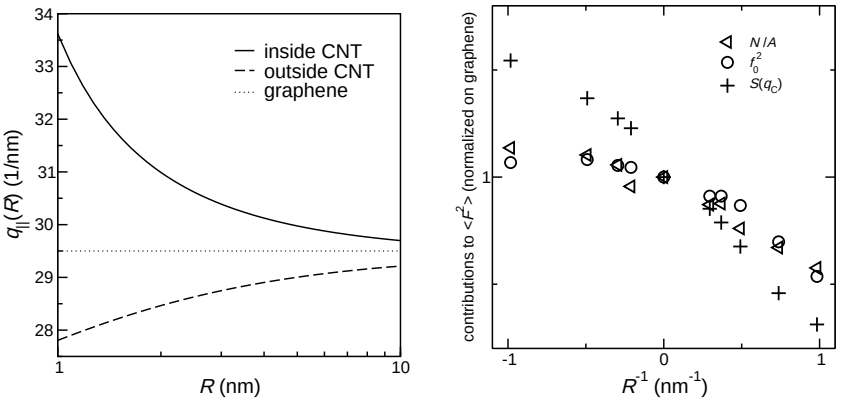

(a) Curvature dependence of $q_{\parallel}$

(b) Contributions to $\langle F^2 \rangle$

Figure 7: Curvature dependence of *(a)* the reciprocal lattice vectors absolute value $q_{\pm} = q_{\parallel}$ (see Eq.(9) and (14)) *(b)* the contact density $\frac{N}{A}$, the force amplitude $f_{q_{\parallel}}$ and the commensurability factor $S(q_{\parallel})$; normalized on the values for graphene (zero curvature)
The commensurability of CNT and water structure is the most important factor for the curvature dependence of the friction coefficient. The change of $S(q_{\parallel})$ is not due to a change in the water structure, but only to the curvature induced change of the potential landscape at the site of the first water layer.

The structure factors for $R = 0.34$, 0.41 and 0.47nm are compared in the inset of Fig.3 in the article. The right side of this figure shows the increase of the first peak for strong confinements. For the single file cases, it exceeds the crystallization criterion $S = 2.85$.

3.1 1D analytical model for structure factor

We note that the structure factor of single file water is in agreement with the model of an infinitely long chain of particles where the nearest neighbors are coupled by springs with spring constant κ at equilibrium distance z_0.

The density of a N-particle chain is given by

$$\rho(z) = \sum_{i=1}^{N} \delta(z_i - z) \tag{16}$$

and the potential energy of the system is

$$V = \sum_j \frac{\kappa}{2} y_j^2 \ . \tag{17}$$

were y_j is the elongation of spring j between particles $j-1$ and j. The structure factor can be expressed as a function of the spring elongations:

$$\begin{aligned} S(q) &= \frac{1}{N} \int_{-\infty}^{\infty} \int_{-\infty}^{\infty} \mathrm{d}z \mathrm{d}z\prime \ \mathrm{e}^{\mathrm{i}q(z-z\prime)} \left\langle \rho(z)\rho(z\prime) \right\rangle \\ &= 1 + \frac{1}{N} \sum_{j=1}^{N-2} \sum_{l=j+1}^{N-1} \left\langle \prod_{m=j+1}^{l} \mathrm{e}^{\mathrm{i}q(y_m+z_0)} + \prod_{m=j+1}^{l} \mathrm{e}^{-\mathrm{i}q(y_m+z_0)} \right\rangle . \end{aligned} \tag{18}$$

With the canonical ensemble average $\left\langle \prod_{m=j+1}^{l} \mathrm{e}^{\pm \mathrm{i}q(y_m+z_0)} \right\rangle = \mathrm{e}^{(l-j)\left(-q^2 k_\mathrm{B} T/2\kappa \pm \mathrm{i}q z_0\right)}$ and the thermodynamic limit $N \to \infty$, the structure factor reads

$$S(q) = \frac{1 - \exp(-q^2 k_\mathrm{B} T/\kappa)}{1 - 2\exp(-q^2 k_\mathrm{B} T/2\kappa)\cos(q z_0) + \exp(-q^2 k_\mathrm{B} T/\kappa)} \tag{19}$$

A fit of this expression on the data for the two smallest tubes (fit parameters κ and z_0) gives the solid lines in the inset of Fig.4 in the article.

3.2 Curvature dependent contributions to the friction coefficient

It turns out that the relation $\left\langle F^2 \right\rangle \sim N f_{q_\parallel}^2 S(q_\parallel)$ also holds true for the one dimensional case of a water chain in the middle of the CNT. This can easily be derived analog to Eq.(6) with the force $f(z) = f_{q_\parallel} \sin(qz)$ and the structure function from Eq.(15) instead of Eq.(13). However, there are several differences in the high confinement regime concerning the influence of these quantities on

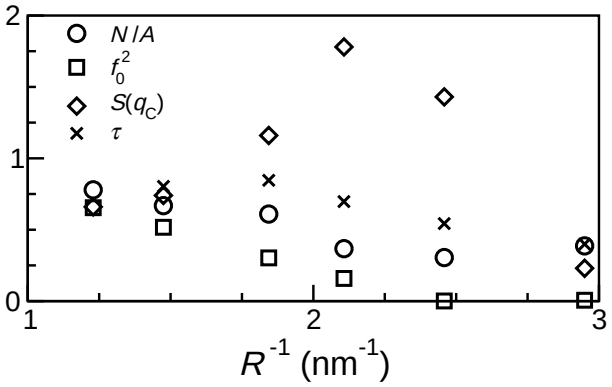

Figure 8: Curvature dependent contributions to the friction coefficient λ in the case of strong confinement (CNT with radii $R < 1$nm): contact density $\frac{N}{A}$, force amplitude $f_{q_\parallel}$, structure coefficient $S(q_\parallel)$ and correlation time τ. All quantities are normalized on the values for graphene (compare Fig.11)
The frictionless flow of single file water is caused by the quasi vanishing roughness of the oxygen-wall potential which means negligible force amplitude $f_{q_\parallel}$.

the friction coefficient. On the one hand, the q-vector of the oxygen-wall potential does not change as in Eq.(14) anymore. On the other hand, the structure factor in z-direction changes drastically with the tube radius due to the increasing confinement. Both facts combined lead to a rather unsystematic behavior of the structural contribution $S(q_\parallel)$. Furthermore, the strong confinement also has an impact on the water dynamics which influences the correlation time τ. But non of this really matters for the friction coefficient as can be seen in Fig.(8). The dominating factor which leads to frictionless motion for single file water is the roughness of the potential.

4 Various tests

4.1 zigzag tubes

Both the roughness of the potential and the reciprocal lattice vector $q_\parallel$ at which the water structure factor $S(q)$ is evaluated, are determined by the CNT structure. In order to test this dependence of the friction coefficient on the wall structure, we performed equilibrium and flow simulations of water in zigzag CNT with radii between 0.35nm and 9.8nm. There is indeed a remarkable influence of the CNT chirality on the friction: In zigzag CNT of $R \lesssim 2$ nm, friction is considerably higher than in armchair CNT of the same size. This difference can be quantitatively understood within the presented theory (compare Fig.9)

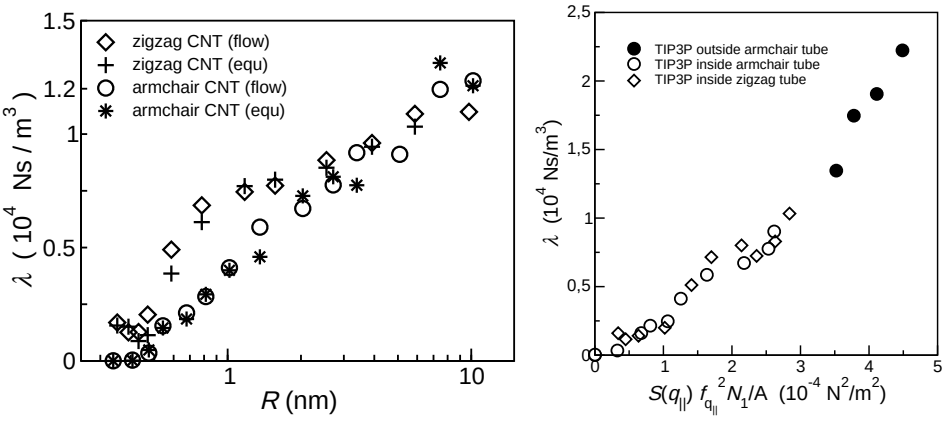

Figure 9: *left*: Friction coefficient of water flowing through zigzag and armchair CNT of varying radius R. The chirality of the CNT has a considerable influence on the friction coefficient. It is higher for zigzag than for armchair CNT of comparable size, especially for $R \lesssim 1.1$nm.
right: Data for the friction coefficient in both zigzag and armchair tubes collapse on the same curve when plotted against the theoretical expectation from Eq. 11 which shows that this expression for the friction coefficient captures all relevant parameters to explain the observed curvature effect

4.2 SPC-E water model

We also performed equilibrium simulations for all system types (water inside/ outside CNT and in graphene slab) with the SPC-E water model. The main difference to the TIP3P water model is the water-graphene contact angle. Simulation of a water droplet on a graphene sheet gave a water-carbon contact angle of $\theta = 95^\circ \pm 2^\circ$ for SPC-E and $\theta = 57^\circ \pm 2^\circ$ for TIP3P. The slightly non-wetting behavior of the SPC-E water caused some problem with the pressure equilibration procedure for water in the CNT as it was described in the beginning. For the combination TIP3P/Amber, the CNT was empty in the starting configuration, but water from the reservoirs immediately began to fill the tube. For SPC-E/Werder parameters, however, a pressure of 1atm is too low to force water into CNT. So, for the friction measurement with SPC-E water inside CNT, we used the same number of particles as for the TIP3P simulations. This means, that these results were certainly obtained at a higher tangential pressure than for SPC-E water outside and in the graphene slab, where the equilibrium number of molecules could be determined without problems. Nevertheless, we think that it's justified to directly compare all these results since the friction coefficient was found to be independent of the pressure in a wide range (Fig.1b).

All results for the two different water models are in qualitative agreement. Quantitatively, the friction coefficient differs up to $\approx 60\%$ (for water outside CNT). In general, friction measured with the SPC-E water model is higher

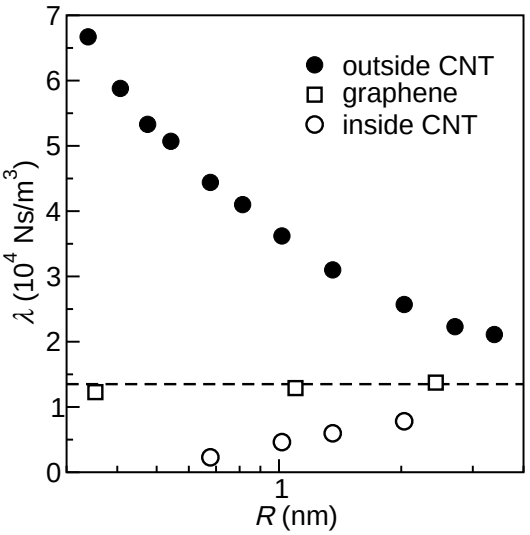

Figure 10: Friction coefficient for water inside and outside armchair CNT with radius R and for water confined between two graphene planes of distance $R/2$, obtained with the SPC-E water model. The dashed line is a guide to the eye.

than for TIP3P.